Available online at www.sciencedirect.com
ScienceDirect
Polymer 48 (2007) 6064–6076
polymer
www.elsevier.com/locate/polymer

Buckling of jets in electrospinning

Tao Han [a], Darrell H. Reneker [a,*], Alexander L. Yarin [b]

[a] Department of Polymer Science, The University of Akron, Akron, OH 44325-3909, USA
[b] Department of Mechanical and Industry Engineering, University of Illinois at Chicago, Chicago, IL 60607-7022, USA

Received 9 July 2007; accepted 2 August 2007
Available online 8 August 2007

Abstract

Various buckling instabilities of electrospinning jets were observed and compared with the buckling instabilities of uncharged fluid jets. Buckling instability arises due to jet compression at impingement on a collector surface and occurs independently of the electrical bending instability. The velocity, diameter, density and viscosity of the electrospinning jets are the key factors that determine the buckling frequency. The electrically charged jets impinging onto grounded, horizontal or inclined (wedge-like) electrodes moving laterally at a constant velocity are studied experimentally. Straight and bending (electrospinning) jets emerge at short and sufficiently long inter-electrode distances, respectively. The experiments show that both straight segment and bending jets, when impinging onto a counter-electrode, buckled and produced patterns of meandering deposits. In the case of bending electrospun jets these short-length buckling patterns were superimposed on the bending loops found in the deposits. Buckling-related and bending-related morphologies are easily distinguishable. The buckling patterns have frequencies of the order of 10^5–10^6 Hz, whereas the bending loops are formed at the frequencies of the order of 10^3 Hz. The deposited buckling patterns include sinuous, zigzag-like, figures-of-eight, recurring curves, coiled and other structures that resembled many patterns created by uncharged jets of highly viscous fluids impinging a hard flat surface. In addition, several new morphologies which were not observed before with uncharged jets were found. The experimentally measured frequencies of the buckling patterns were compared to the theoretical predictions and a reasonable agreement was found.

Keywords: Electrospinning; Buckling instability; Nanofibers

1. Introduction

Buckling of highly viscous Newtonian liquid jets was studied experimentally in the seminal work of Taylor [1]. He assumed that buckling of a liquid jet results from the compressive force imposed by an obstacle the jet impinges upon or a distributed compressive force imposed by an environment. In this sense buckling of liquid jets is kindred to the classical buckling of compressed elastic bars and columns discovered by Euler [2]. Further experiments on buckling of highly viscous liquid jets were published in Refs. [3,4]. The explanation that buckling of liquid jets and films is caused by longitudinal compressive forces was fully confirmed in the framework of the detailed theoretical analysis based on the quasi-one-dimensional equations of dynamics of liquid jets [5–7]. In all the above-mentioned works jet buckling occurred when a jet impinged on motionless surfaces or liquid–liquid interfaces. Recently jet buckling on laterally moving solid surfaces nearly perpendicular to the jet axis was reported in Ref. [8]. The stability analysis in that case was also based on the quasi-one-dimensional equations of dynamics of liquid jets similar to [5–7] and revealed that characteristic frequencies of buckling are practically unaffected by the lateral motion of the surface and stay the same as in the case of collection of a liquid jet on a stationary hard flat surface [9].

In the papers cited above the liquid jets were not electrified and patterns evolved only under the action of forces of mechanical origin. In electrospinning, jets of viscoelastic polymer solutions evolve primarily under the action of the electric forces. In particular, electrified jets experience the

* Corresponding author. Tel.: +1 330 294 6949; fax: +1 330 294 5290.
E-mail address: reneker@uakron.edu (D.H. Reneker).

0032-3861/$ - see front matter © 2007 Elsevier Ltd. All rights reserved.
doi:10.1016/j.polymer.2007.08.002

bending instability that is driven by the mutual repulsion of the excess electric charges carried by electrospun jets [10–12], as well as (sometimes) a secondary branching also rooted in charge repulsion [13]. The present work reports the observation of the deposited fibers resulting from the electrospun jets that were coiled by the electrical bending instability, as well from the straight segment of electrically driven jets which impinged onto a collector surface before electrical bending occurred (some preliminary results were reported in conference proceedings [14]). The effects of the laterally moving collector surfaces were observed. Buckling may or may not accompany bending instability of electrospun jets, but in fact, represents a totally different and distinguishable phenomenon that occurred very close to the collector.

Section 2 describes the experimental setup and materials used. Section 3 contains the experimental results. Discussion is presented in Section 4. Conclusions are drawn in Section 5.

2. Experimental

2.1. Materials

Polyethylene oxide, PEO, $M_w = 400$ kDa, 6 wt% solution in deionized water; poly(L-lactide), PLLA, $M_w = 152$ kDa, 5 wt% solution in hexafluoroisopropanol, HFIP; polystyrene, PS, $M_w = 350$ kDa, 25 wt% in dimethylformamide, DMF; nylon-6, 25 wt% solution in formic acid, FA, (88%); nylon-6, 10 wt% solution in HFIP/FA mixture with the HFIP/FA ratio being 8:2 (by weight). Nylon-6, poly(L-lactide) and all solvents were purchased from Sigma-Aldrich Co. Polystyrene and polyethylene oxide were purchased from Scientific Polymer Products, Inc. and used as received.

2.2. Experimental setup

The experimental setup for electrospinning was similar to those used previously [10–13]. However, the grounded collector might be tilted at different angles from $\theta = 0$ to 45°. (Fig. 1). The collector might be either motionless or move horizontally at a constant speed of typically $V_c = 0$–3 m/s. Also, in some experiments a grounded liquid surface was used as collector. When the lateral moving inclined collector was used, the lateral motion of the collector was in the direction that caused the separation between the tip and the collector to increase.

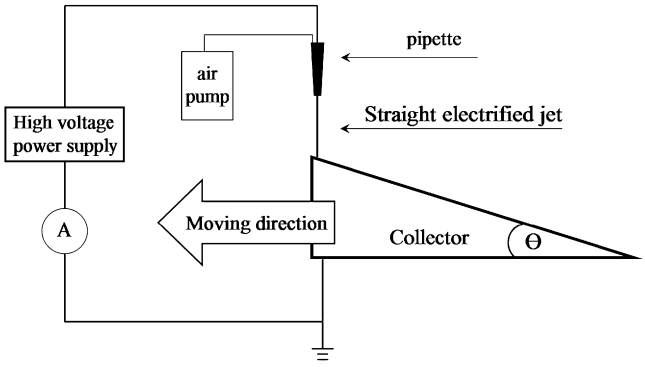

Fig. 1. Sketch of the experimental setup. Permission from Materials Research Society (requested July 9, 2007).

The experiments were conducted under ambient conditions at room temperature and relative humidity of about 25%. Polymer solutions were held in a glass pipette which had a 2 cm long capillary at one end. The inner diameter of the capillary was 160 μm. A copper wire was immersed in the solution and connected with a high voltage power supply which could generate DC voltage up to 13 kV. No syringe pump was used, and the flow was controlled by the outward electric pressure and the air pressure or partial vacuum applied to the surface of the liquid in the pipette. The distance between the capillary and the collector along the straight vertical line could be adjusted from 0.1 to 100 cm. An ammeter was connected between the wedge-like collector and electrically grounded wire to measure the current carried by the straight or electrospinning jets.

2.3. Characterization

Collected solidified electrospun fibers were observed with optical microscopy (Olympus 51BX) and Scanning Electron Microscopy (JEOL 5310).

3. Experimental results

Figs. 2 and 3 are images of two electrically driven jets sufficiently above the collecting surface. In the case of a short (for

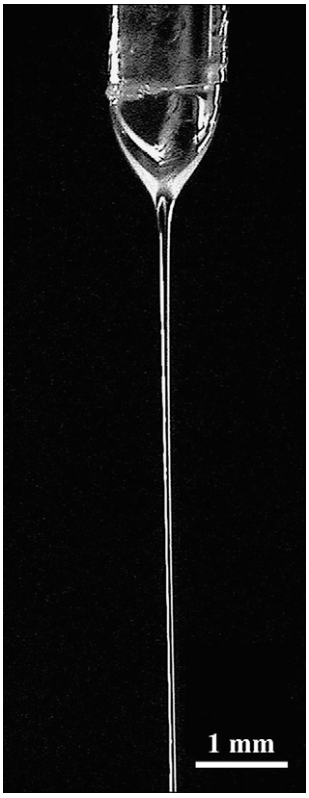

Fig. 2. Straight electrified jet, too short to develop an electrical bending instability. Permission from Materials Research Society (requested July 9, 2007).

Fig. 3. A snapshot of an electrospinning jet with well-developed loops appearing after the onset of the electrical bending instability at some distance from the nozzle. Some short segments of the continuous jet were not illuminated, and therefore are not seen.

a particular polymer solution) nozzle-collector distance the jet is typically straight (Fig. 2), whereas at a longer distance (for the same solution) the jet length was sufficiently long for the electrical bending instability to occur (Fig. 3).

3.1. Buckling of straight electrified jets: PEO solution collected on a horizontal moving grounded plate

The PEO solution, held in the pipette, was connected to high voltage power supply. The distance from the capillary orifice to the horizontal grounded collector was 1 cm. The horizontal collector was moved sideways at $V_c = 0.785$ m/s. The voltage was 2 kV. Under these conditions, the electrical bending instability did not occur and only a straight electrified jet was observed. In this case the relative velocity between the jet and collector V_r was equal to V_c, since straight jets did not move sideways prior to buckling. The buckled patterns collected were observed using scanning electron microscopy. Fig. 4 shows the collected buckled PEO fibers. Sinuous folding, zigzag folding and helical coiling occurred. The rate at which the periodic patterns were created was determined from the known velocity of the substrate. The product of the frequency of the buckling instability and the distance advanced by each cycle (λ, wavelength of the deposited buckling pattern) is equal to the relative velocity between the oncoming jet and moving collector. The wavelengths (λ) of the buckled patterns were around 5 μm. The corresponding frequencies ($\omega = V_r/\lambda$) were around 3.42×10^5 Hz. The morphologies of the buckled patterns found in the case of a straight electrified jet resemble those found for buckling of uncharged rectilinear jets impinging on moving plates [8,9].

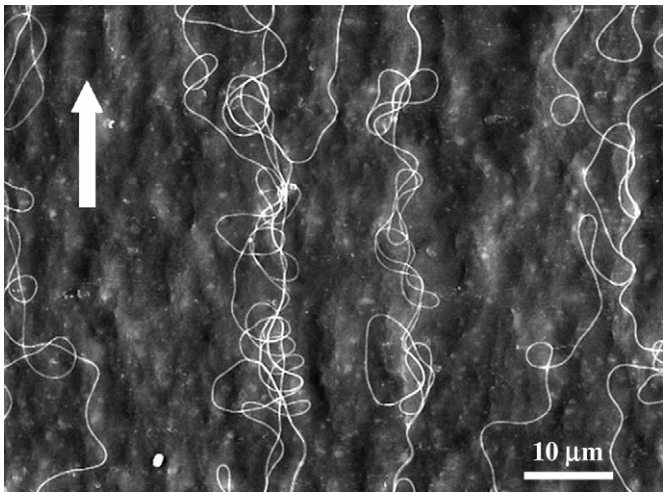

Fig. 4. SEM image of some of the buckled PEO patterns collected on the horizontal collector which was moving at 0.785 m/s along the direction showed by the white arrow.

3.2. Buckling of bending electrospun jets: PEO solution collected on a horizontal moving grounded plate

The deposits resulting from the bending and buckling electrospun jets are shown in Fig. 5. It is emphasized that they clearly demonstrate the difference between the effects of bending and buckling. The patterns associated with bending are the large loops corresponding to frequencies of the order of 10^3 Hz as in Ref. [10]. The buckling-related patterns appear as tiny wiggles that occurred at frequencies of the order of 10^5–10^6 Hz.

The horizontal grounded collector was moving laterally at 0.01 m/s along the direction of white arrow in Fig. 5a. The distance from the tip to collector was 1.5 cm (Fig. 5a and b) and 5 cm (Fig. 5c and d), respectively. At these conditions, electrical bending of the jets occurred prior to impingement onto the collector surface. The diameters of the bending loops at 1.5 cm inter-electrode distances ranged from 100 μm to several millimeters. The diameters of the bending loops at 5 cm inter-electrode distances were several centimeters. Fig. 5a–d also show that the bending loops buckled when they impinged onto the collector surface. The buckling patterns were densely piled along the path of the bending loops. The wavelengths of the buckling patterns were around 15 μm. Here, as before, we define the wavelength as the distance between adjacent identical segments of the repeating patterns. Fig. 5a and b show the wavelengths of the buckling patterns were several μm. The buckling patterns, figure-eights and small circles, were densely piled along the bending loops. Fig. 5c and d show that the wavelength of the buckling patterns in the wiggles were around 15 μm. The buckling patterns were loosely distributed along the bending loops, producing again sinuous waves, figure-eights and small circles. Some of the segments of bending circles in Fig. 5d were not buckled, probably because some parts of the bending circles landed in the way that there was no compressive force along them (a tangential landing), or because these segments solidified before they landed.

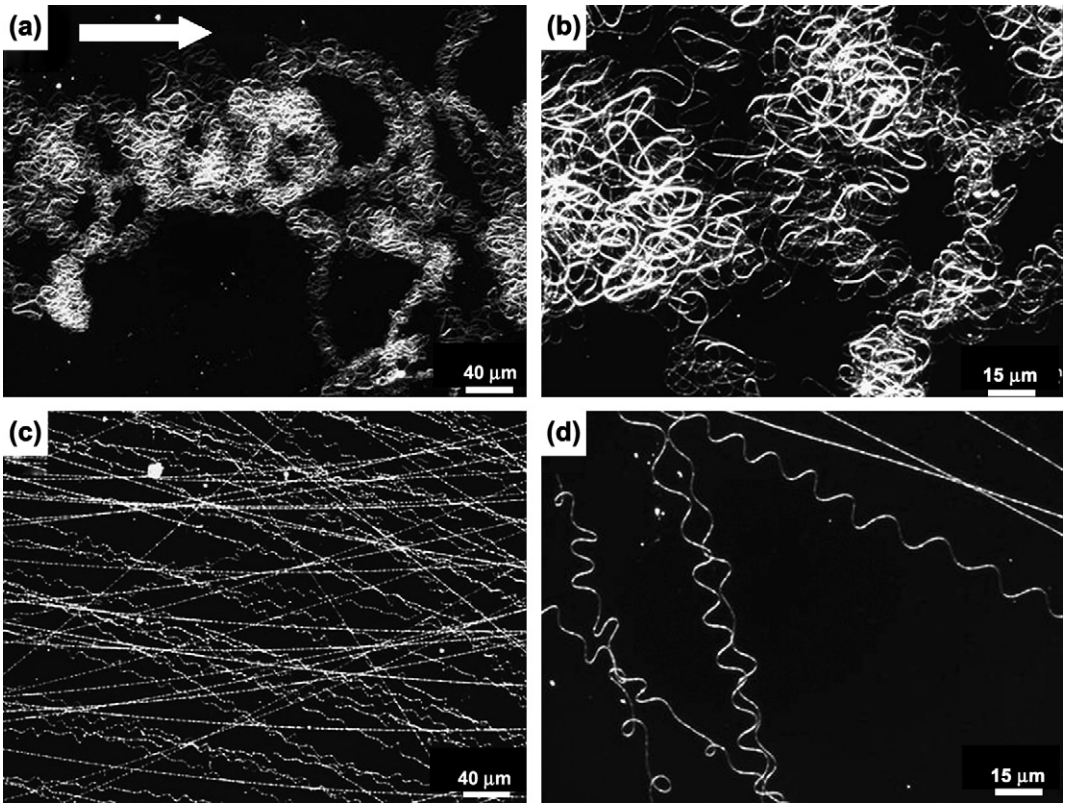

Fig. 5. Optical micrographs of buckled bending electrospun PEO jets.

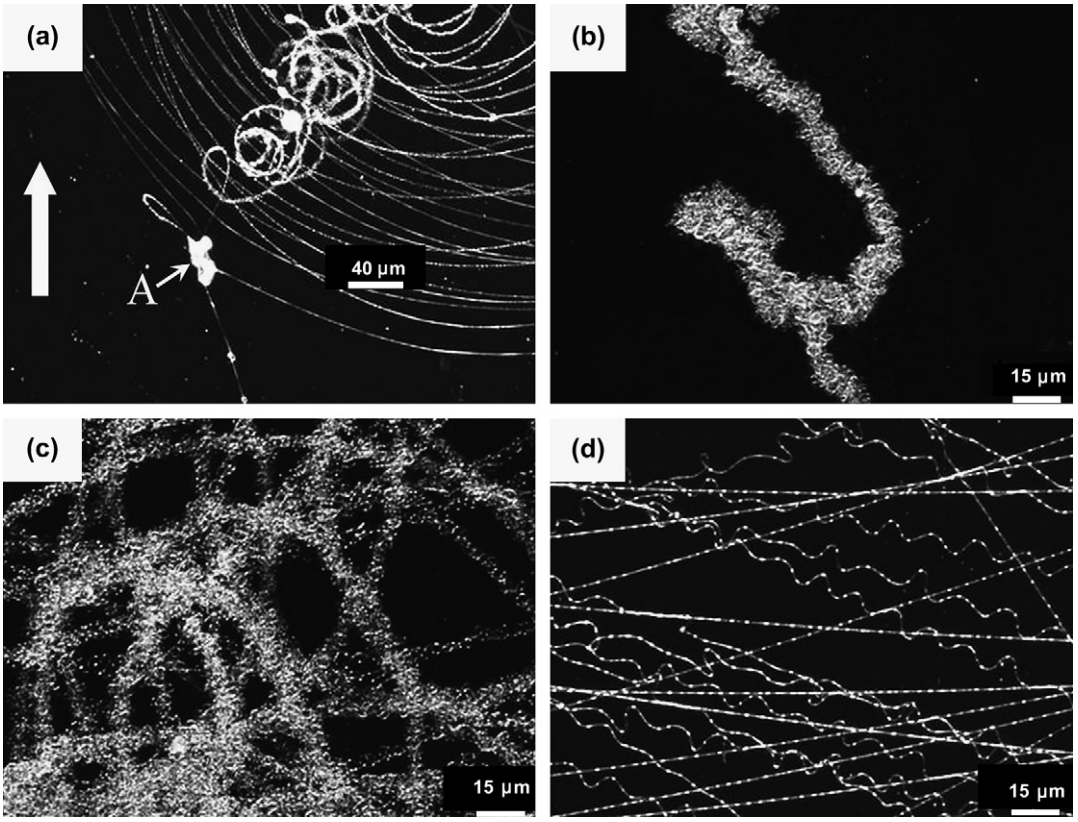

Fig. 6. Optical micrographs of bent and buckled PEO loops and patterns collected at different inter-electrode distances on the surface of a moving and inclined collector. In all images the wedge moved at 0.01 m/s along the direction shown by the white wide arrow in Fig. 6a.

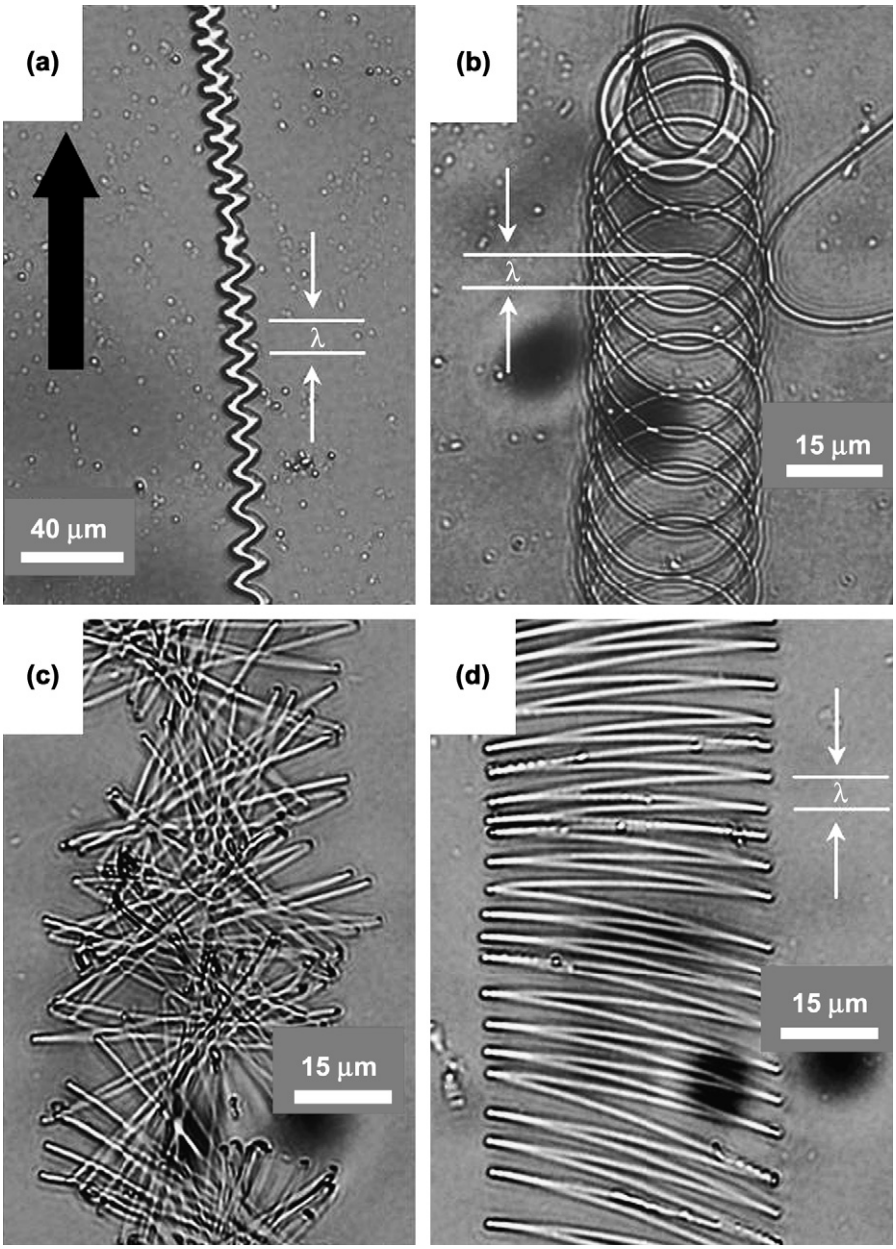

Fig. 7. Optical images of buckled solidified PLLA patterns. In all images the horizontal collector was moved in direction shown by the black arrow in Fig. 7a. The distance λ (the wavelength) corresponds to the lateral motion during one period of the formation of the buckling patterns. Permission from Materials Research Society (requested July 9, 2007).

3.3. Buckling of bending electrospun jets: PEO jets onto an inclined moving collector

A moving grounded collector wedge with an inclination of $\theta = 5^\circ$ was used to collect electrospun PEO jets electrically bent into coils which buckled at the collector. The voltage between the spinneret and collector was 3 kV. Since the inter-electrode distance increased with time due to the lateral motion of the inclined collector, different features of the electrical bending circles and buckling patterns were collected along the slope of the moving collector (Fig. 6).

Fig. 6a shows the large-scale loops originating from the electrical bending instability corresponding to a relatively short inter-electrode distance. The fluid jet accumulated into a droplet near point A in Fig. 6a as the motion started, and then deposited small bending circles which buckled on a scale that can barely be seen in Fig. 6a. The bending circles rapidly became larger in diameter and the piled rows of buckling patterns formed the patterns shown in Fig. 6b. This figure details the buckling patterns superimposed on the very first bending loops. Fig. 6c shows the bending loops with the superimposed buckling patterns corresponding to the intermediate inter-electrode distances. Fig. 6d shows the bending loops with the superimposed buckling patterns corresponding to the largest inter-electrode distance. The above-mentioned figures demonstrate that the buckling frequency and wavelength both vary

with the inter-electrode distance. This results from the fact that as the inter-electrode distance increases, the impinging jet becomes thinner, acquires a higher velocity, and has different rheological parameters, due to solvent evaporation. So the buckling frequency is higher at shorter collecting distances and lower at larger distances. As a result, the piled buckling patterns were more densely packed at the shorter inter-electrode distances and more loosely packed at the larger distances.

3.4. Buckling of straight electrified jets: PLLA jets collected on a horizontal moving grounded plate

A PLLA solution described in Section 2 was used. The distance from the capillary orifice to the grounded collector was 2 cm. The collector was moved laterally at 1 m/s. The applied voltage was 1.5 kV. Under these conditions, for this particular polymer solution the electrical bending instability did not occur and the path of the jet toward the collector was straight. Near the collector the jet buckled. The deposited and solidified buckled patterns collected on glass microscope slides were observed using optical microscopy. The charge carried by the jet was quickly relaxed due to the surface conductivity of the glass. Fig. 7 shows the solidified buckled patterns produced from the straight PLLA jet. The diameters of the solidified PLLA fibers were around 1–2 μm. Sinuous patterns are shown in Fig. 7a and helical patterns are shown in Fig. 7b. Zigzag with straight segments only about 45 μm long were found in twisted rows, Fig. 7c and in flat arrays, Fig. 7d.

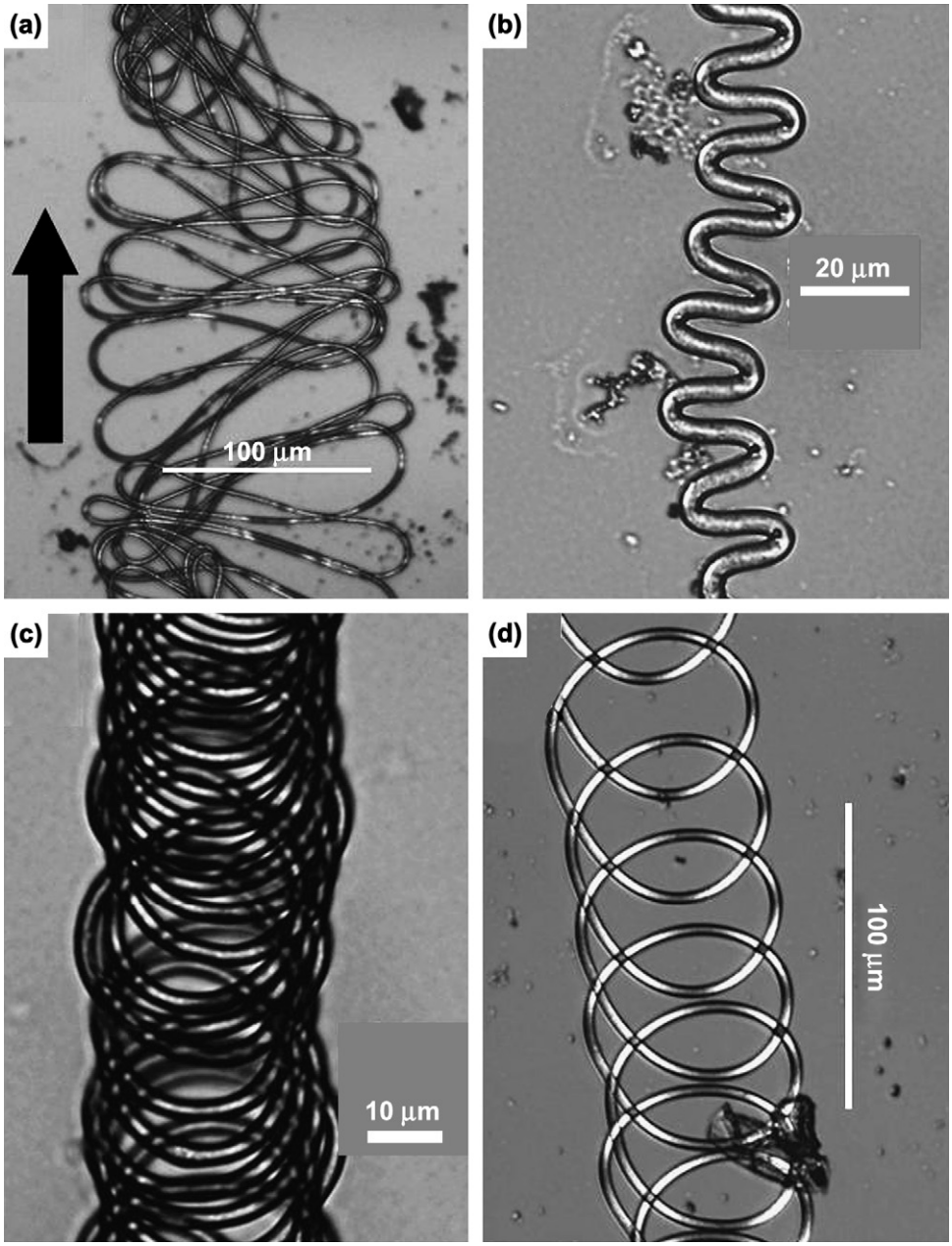

Fig. 8. Optical micrographs of buckled polystyrene patterns. The horizontal collector was moved in the direction shown by the black arrow in Fig. 8a.

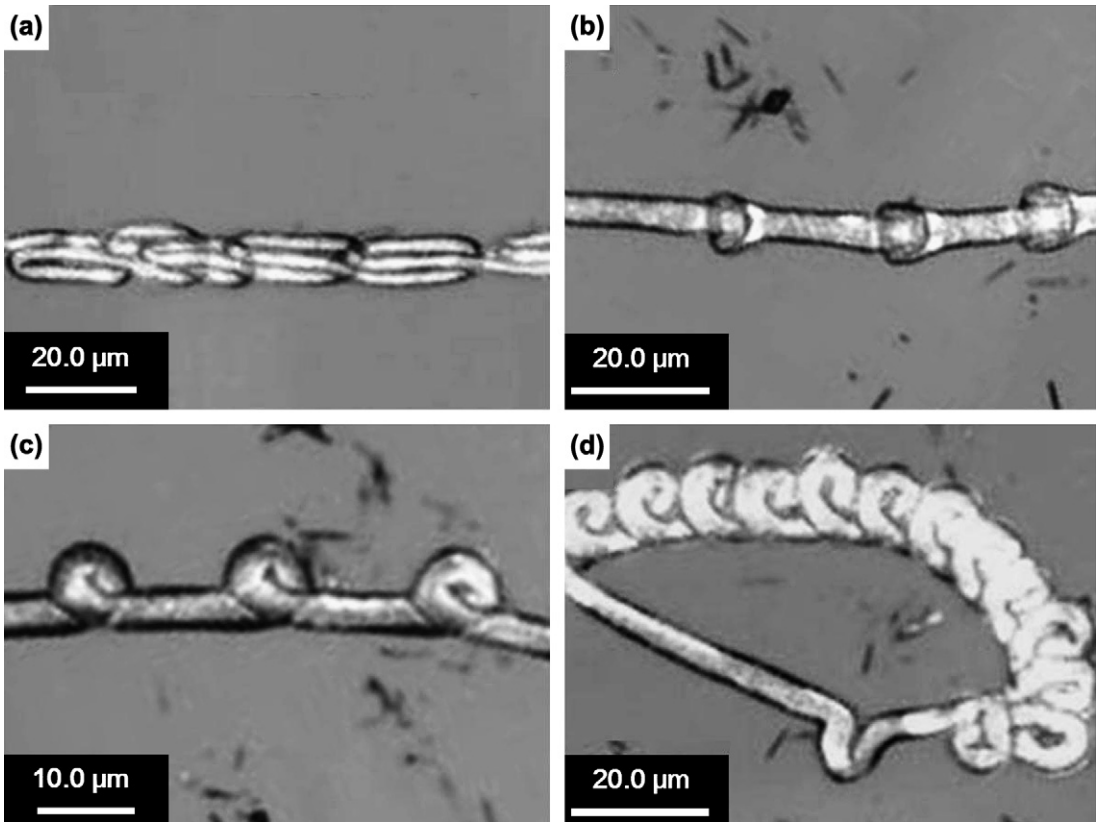

Fig. 9. Optical micrographs of buckled polystyrene patterns collected on a static water surface.

For such patterns the micrographs allow measurement of the corresponding wavelength λ (cf. Fig. 7a, b and d). The measured wavelengths were around 6–12 μm. The corresponding frequencies ω defined as $\omega = V_r/\lambda$ (with V_r being the lateral velocity of the collector V_c, since the straight jet did not have any lateral motion of its own) were around 0.83×10^5–1.67×10^5 Hz. In some cases (Fig. 7c) the buckled deposits were rather chaotic, so that it was impossible to ascribe them to any λ. The buckling patterns produced by the straight electrified jets resemble those found for buckling of uncharged rectilinear jets impinging on moving plates [8,9].

3.5. Buckling of straight electrified jets: polystyrene jets onto a horizontal moving grounded plate

The polystyrene solution described in Section 2 was used. The distance from the tip to the collector was 2 cm. The collector was moved laterally at 2 m/s. The voltage was 3 kV. Under these conditions, the electrical bending

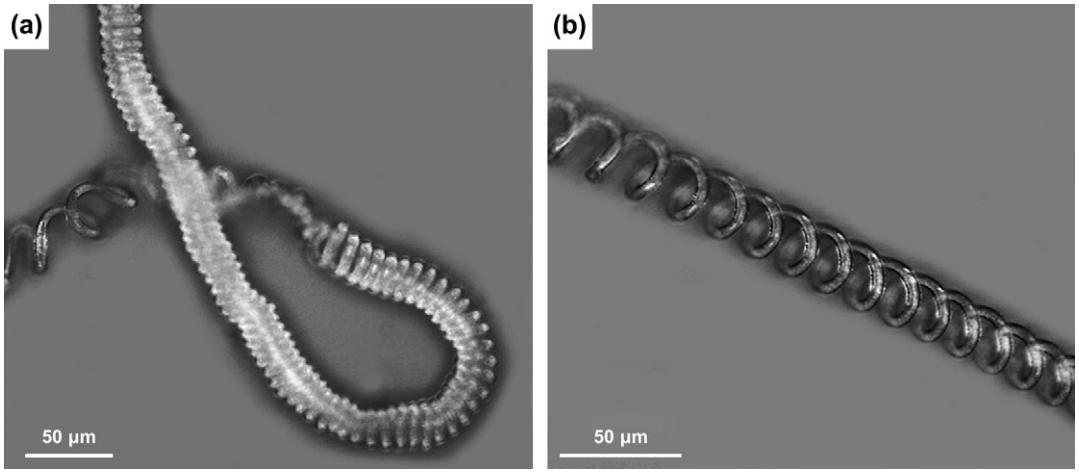

Fig. 10. Three-dimensional buckled patterns formed after the impingement of a polystyrene jet onto a water surface. The samples were dipped from the water with a glass microscopic slide and observed with the optical microscopy.

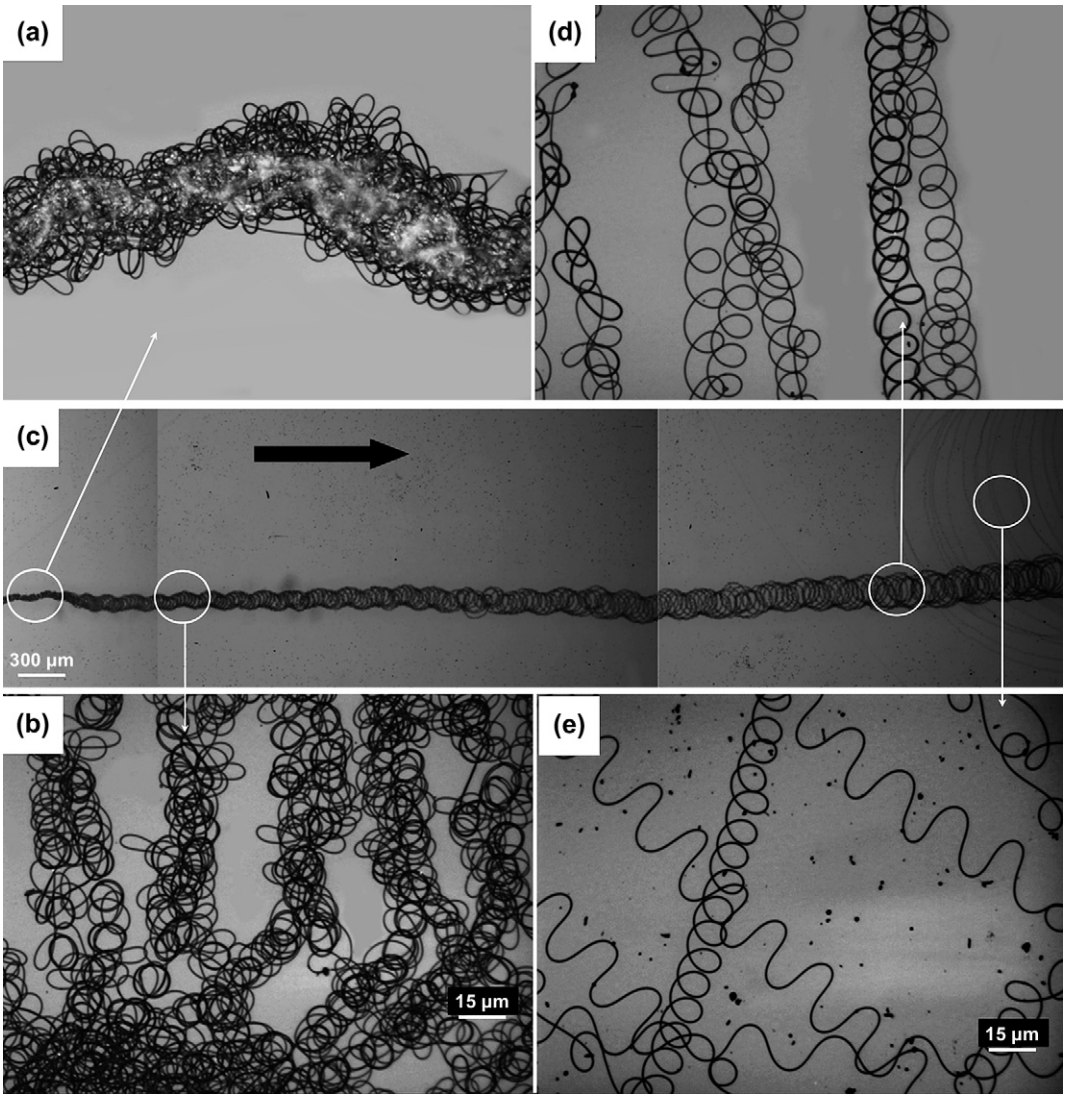

Fig. 11. Buckled and bent electrospun nylon-6 deposits. The lengths of the horizontal edges of the images a, b, d, e are 0.18 mm; the length of the horizontal edge of the image c is 6.0 mm. The total change in the inter-electrode distance was about 0.3 cm from the left edge to the right edge in Fig. 11c. Permission from Materials Research Society (requested July 9, 2007).

instability did not occur and only a straight jet was observed. The axial velocity of the jet was around 2 m/s before it impinged onto the collector surface. The solidified buckled patterns collected on a glass slide were observed using optical microscopy. Figs. 8 and 9 show the patterns observed on buckled polystyrene jets. The diameters of the jets were around 2–6 μm. Figure-eight (Fig. 8a), sinuous folding (Fig. 8b), helical coiling (Fig. 8c) and overlapping script-like "e" (Fig. 8d, Fig. 9c and d) were observed. Also "paper clip chain" (Fig. 9a), and "knee-like" (Fig. 9b) patterns were formed under some circumstances. The wavelengths were measured from the micrographs and were found to be around 6–30 μm. The corresponding frequencies were around 0.67×10^5–3.3×10^5 Hz.

In some experiments a stationary water surface was used as a collector. The straight jet buckled as it impinged onto the surface and then sank into the water. Three-dimensional buckling morphologies were shaped as a coiling spring (Fig. 10). The diameter of the three-dimensional coil was around 20 μm.

3.6. Buckling of bending electrospun jets: nylon-6 onto an inclined moving collector

A moving collector with an inclination of $\theta = 18.5^\circ$ was used to collect electrospun jets of nylon-6 (10 wt% in an 8:2 mixture of HFIP and FA). The simultaneous evolution of the electrical bending and buckling was observed, see Fig. 11. The direction of the collector motion is shown by the bold black arrow in Fig. 11c. Since the inter-electrode distance increased from about 0.1 to about 7.5 cm with time due to the motion of the inclined collectors, different patterns were observed along the collector surface (Fig. 11). Fig. 11c is an overall view of the deposited fiber along the wedge slope. Four sections of the overall view are enlarged in Fig. 11a, b, d and e as is shown by white arrows in Fig. 11. The nearly

straight segment of the jet formed a complex, sinuous network of smaller loops, as shown at higher magnification in Fig. 11a. At a larger inter-electrode distance, the bending instability produced loops 200 μm in diameter with superimposed, much smaller, buckling patterns that were 15 μm in diameter, as is seen in Fig. 11b and Fig. 11d. Near the right edge of Fig. 11c, parts of larger coils formed by the electrical bending were observed. The enlarged image shown in Fig. 11e shows coils and sinuous patterns caused by buckling. Fig. 11c shows that the buckling instability occurred both before and after the electrical bending instability developed, and produced coils or sinuous patterns with diameters a little less than 15 μm, in the region shown in Fig. 11a and a little more than 15 μm in the region shown in Fig. 11e.

4. Discussion

The experimental data presented in Section 3 shows that the deposited buckling patterns of the electrified jets have reproducible characteristics that are similar to those found previously in uncharged jets collected by impingement on a moving hard flat surface [8,9] irrespective of whether the electrically driven jet was straight or bent prior to interaction with the collector. Similarities between charged and uncharged buckling jets are clearly apparent (cf. Figs. 12 and 13 for polyethylene oxide and nylon-6, respectively). For the uncharged jets it was shown that the characteristic buckling frequency is not significantly dependent on the velocity of lateral motion of an obstacle, being in fact the same as for a motionless collector [9]. Therefore, the predicted buckling frequencies for the impingement of the uncharged jet onto a motionless plate [5] can be directly compared with those measured for a charged jet impinging on a moving collector in the present work. The theoretical results for the buckling frequency are shown in Fig. 13b in Ref. [5]. They may be fitted by the following formula:

$$\log\left(\omega\frac{d}{V}\right) = -0.0194\log\left(\frac{\mu Q}{\rho g d^4}\right) + 0.2582 \tag{1}$$

where ω is the buckling frequency in Hz, d is the jet diameter, V is the jet velocity normal to the collector, Q is

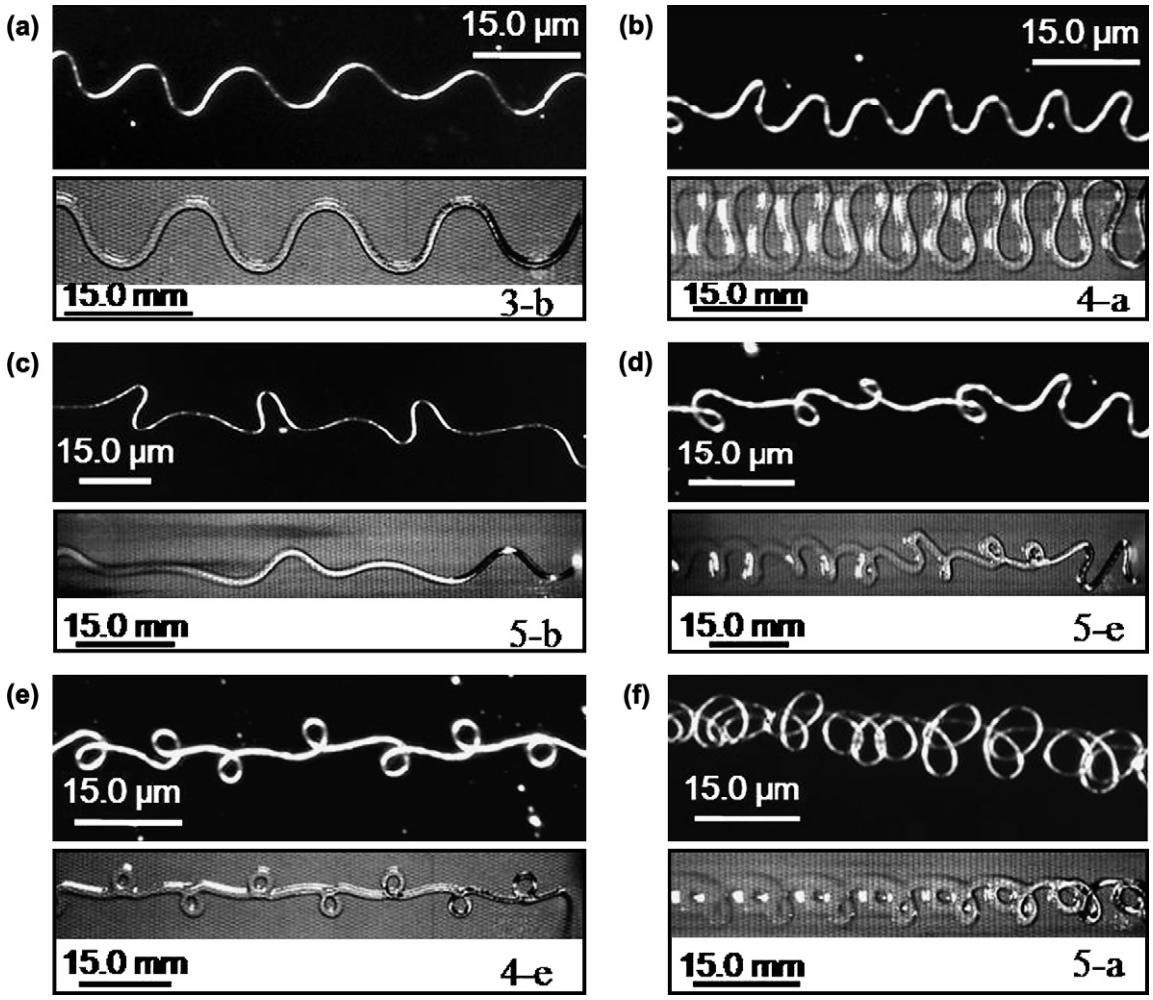

Fig. 12. a–f: Comparison of the buckled patterns created by electrified jets of polyethylene oxide in water, collected on glass slides, to patterns [8] produced by the buckling of uncharged gravity-driven syrup jets. Note that the gravity-driven syrup jets and their buckling patterns are about 1000 times larger than those of the electrified jets of polyethylene oxide in water. The upper panel in each pair depicts the results for the electrified PEO jets in the present work. The lower panel shows the similar patterns by the syrup jets in Ref. [8]. The symbols in the lower right corner of each panel are the figure number found in Ref. [8].

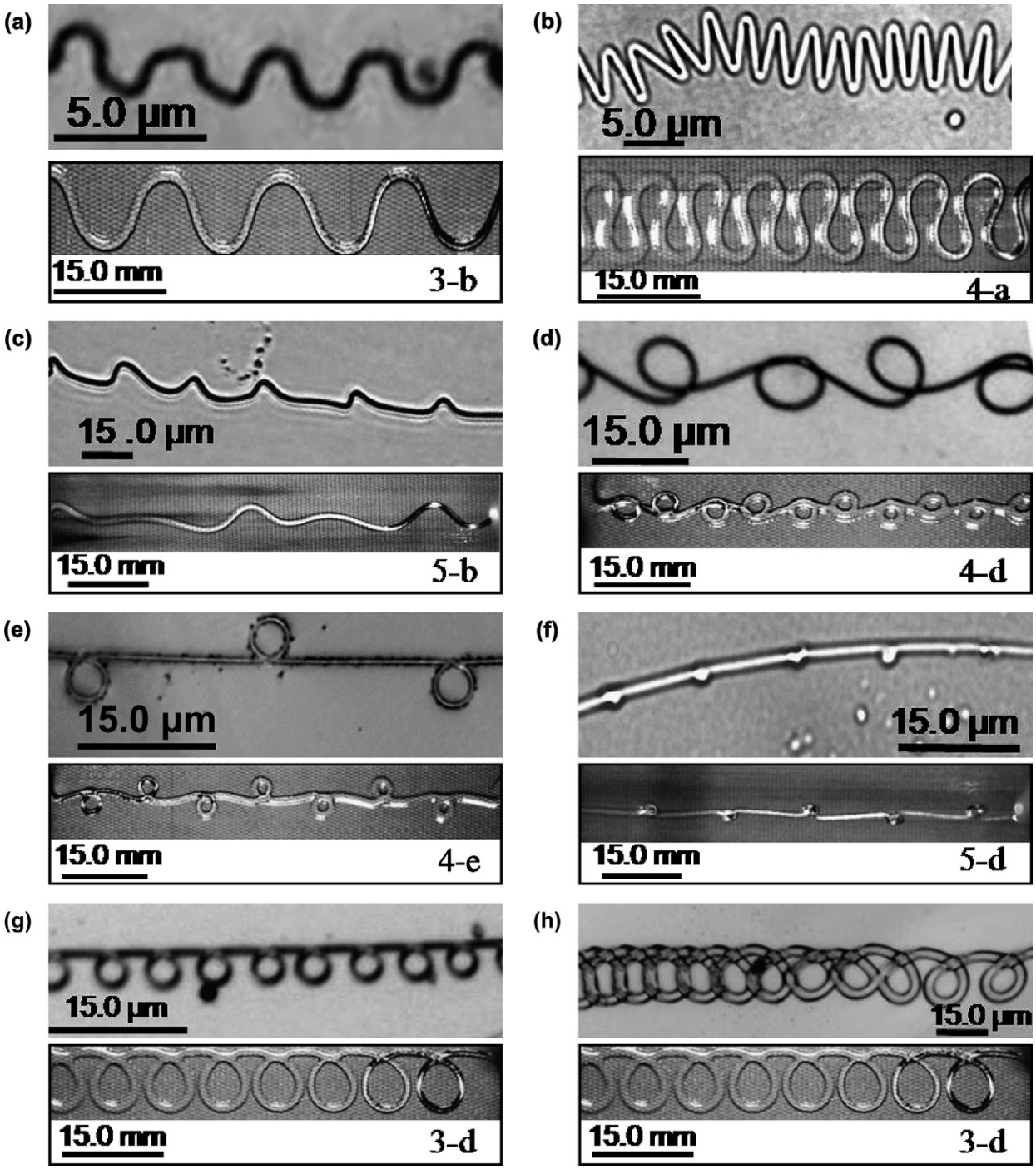

Fig. 13. a–h: Comparison of the buckled patterns created by electrified nylon-6 jets collected on water to the buckling patterns [8] resulting from uncharged gravity-driven syrup jets.

volumetric flow rate in the jet, ρ and μ are the density and viscosity of the liquid. In the present context g is the external force per unit mass (the electric force per unit mass). Buckling is a low-speed and low-strain-rate phenomenon. Therefore, in this limit viscoelastic behavior reduces to Newtonian behavior with μ being equivalent to the zero-shear viscosity.

In the comparison below, d and V in Eq. (1) were evaluated for the segment of the jet near the collector, and used to find $\omega_{\text{calculated}}$ using the other parameters corresponding to specific experiments. In addition, the values of ω_{measured} were independently measured using the deposited patterns, as described in Section 3. Comparisons of $\omega_{\text{calculated}}$ and ω_{measured} are presented in Table 1 with data from Figs. 4–14 for polyethylene oxide, PLLA, polystyrene and nylon-6. Eq. (1) was used to calculate the values of $\omega_{\text{calculated}}$ in all the cases. It is emphasized that the values $\log(\omega(d/V))$ and $\log(\mu Q/\rho g d^4)$ for the electrified jets in the present work extrapolate outside the

Table 1
Comparison of the measured and calculated buckling frequencies for electrospun jets

Figure number	Diameter of the fiber (d) μm	Wavelength (λ) μm	Cycles/mm	Frequency (ω) 10^5 Hz		Fiber length per cycle[c] μm	Velocity of the collector m/s
				Measured	Calculated		
4	0.2	5	200	3.4	7.0	23	0.785
5a	0.3	5	200	2.0	4.7		
5b	0.3	5	200	2.0	4.7		
5c	0.2	15	67	2.7	28.0	25	4.00[a]
5d	0.2	15	67	2.7	7.0	25	4.00[a]
6c	0.3	5	200	2.0	4.7		
6d	0.2	15	67	2.7	7.0	18	4.00[a]
7a	3.8	14	71	0.7	0.4	25	1.00
7b	1.0	7	143	1.4	1.4	82	1.00
7c	1.0	1.5	667	6.7	1.4	60	1.00
7d	1.1	4.8	208	2.1	1.3	60	1.00
8a	2.4	17	59	1.2	1.2	334	2.00[b]
8b	3.9	12.3	81	1.6	0.7	41	2.00[b]
8c	2.4	3.2	312.5	6.2	1.2	52	2.00[b]
8d	2.4	30	33	0.7	1.2	100	2.00[b]
9a	2.7	12	83	1.7	1.0	79	2.00[b]
9b	4.4	23	43	0.9	0.6	31	2.00[b]
9c	3.9	18.5	54	1.1	0.7	44	2.00[b]
9d	4.4	9	111	0.2	0.6	36	2.00[b]
10a	6.4	8	125	2.5	0.4	73	2.00[b]
10b	6.4	8	125	2.5	0.4	73	2.00[b]
11b	0.45	2.6	385	3.8	6.2	31	1.00[a]
11d	0.4	8.5	118	5.9	7.0	35	5.00[a]
11e	0.35	20.2	50	5.0	8.0	45	10.00[a]
12a	0.2	13	77	1.5	3.5	19	2.00[a]
12b	0.2	8.4	119	2.4	3.5	17	2.00[a]
12c	0.2	30.6	33	6.5	3.5	46	2.00[a]
12d	0.2	12	83	1.7	3.5	19	2.00[a]
12e	0.2	10	100	2.0	3.5	19	2.00[a]
12f	0.2	4.2	238	4.8	3.5	21	2.00[a]
13a	0.3	3.4	294	5.9	9.3	5.3	2.00[a]
13b	0.8	2.4	417	8.3	3.5	11	2.00[a]
13c	1.2	23	43	0.9	2.3	26	2.00[a]
13d	0.7	21	48	1.0	4.0	49	2.00[a]
13e	0.5	20	50	1.0	5.6	33	2.00[a]
13f	1.2	12	83	1.7	2.3	14	2.00[a]
13g	0.9	5	200	4.0	3.1	10	2.00[a]
13h	2.6	11	91	1.8	1.1	44	2.00[a]
14a	1.2	3.2	312	6.2	2.3	10	2.00[a]
14b	1.2	5.4	185	3.7	2.3	15	2.00[a]
14c	1.0	8.3	120	2.4	2.8	10	2.00[a]
14d	1.3	10	100	2.0	2.2	11	2.00[a]
14e	0.45	1.2	833	16.7	6.2	6	2.00[a]
14f	0.45	2.5	400	8.0	6.2	8	2.00[a]

[a] V_r: the radial velocity of a typical segment of an electrical bending coils relative to the collector. The value was determined from the high frame rate video.
[b] V_c: the velocity of the collector relative to the straight electrified jet.
[c] Fiber length per cycle is defined as the distance along the path of the jets between adjacent identical segments of the repeating patterns.

range covered by the theoretical data [5] fitted by Eq. (1). Nevertheless, the comparisons in Table 1 show reasonable agreement between the predictions based on Eq. (1) and the current experimental data. Figs. 12 and 13 show that most of the buckling morphologies found in the present work, for the electrified jets, have their counterparts in those for much larger uncharged, gravity-driven jets in Refs. [8,9]. However, there are several other morphologies (Fig. 14), which were not observed before.

Several morphological structures reported in Refs. [15,16] can be attributed to buckling of bending electrospun jets. However, in these works the real origin of the observed deposits was not uncovered. Ref. [15] claimed that such deposit morphologies could not be obtained with non-conducting polymer nanofibers landing on non-metal substrates, and thus attributed them to the competition of charge relaxation and viscoelasticity. The claim was found to contradict to the data in Ref. [16], as well as it does not agree with the results of the present work where one of the non-conducting polymers, PEO, was the same as in Ref. [15]. On the other hand, Ref. [16] attributed the microscale coiled deposits to the ordinary bending instability, while considering

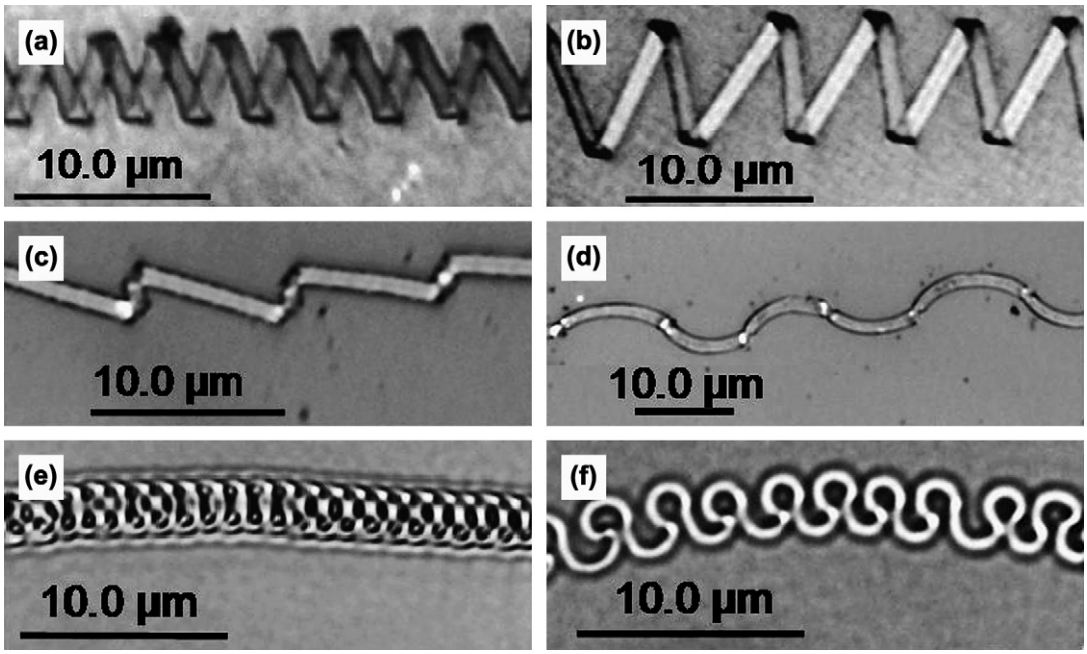

Fig. 14. a–f. Buckled patterns created by electrified nylon-6 jets collected on a water surface. These do not have analogies among those reported in Refs. [8,9].

macroscopic segments as straight. However, in reality the macroscopic segments are coiled (due to the bending instability) with a much larger radius of curvature. The distinctions between the microscopic and macroscopic coils are clearly demonstrated in the present work, and their different physical nature is attributed to two physically different phenomena – mechanical buckling and the electrical bending, respectively.

5. Conclusion

Two- and three-dimensional buckling phenomena were studied in electrically charged jets impinging onto collectors moving laterally at a constant velocity. At short inter-electrode distances the electrified jets were straight, whereas at larger distances the jets developed electrical bending coils characteristic of electrospinning. Both straight and electrically bent jets buckled near the contact with the collector and produced buckling patterns on the collector. In the case of bending electrospun jets the short wavelength buckling patterns were superimposed on the long wavelength electrical bending loops. The frequency range corresponding to the buckling patterns was of the order of 10^5–10^6 Hz, whereas the frequency range for the bending loops was of the order of 10^3 Hz. Most of the morphologies (but not all) of the deposited buckling patterns resembled the patterns produced by uncharged, highly viscous, gravity-driven jets impinging onto a moving hard flat surface published recently [8]. Measured frequencies derived from observations of the buckling patterns were compared to those predicted for uncharged jets impinging on a motionless hard flat surface. A reasonable agreement of the theoretical and experimental results was found. To conclude, the morphologies of the electrospun fibers can be manipulated by controlling the buckling instability of the electrospinning jets. Various two-dimensional and three-dimensional micron size patterns have been produced by the buckled electrospun fibers.

Acknowledgement

We acknowledge financial support from the National Science Foundation, DMI-0403835-2 (NIRT), NSF subcontract 25-1110-0038-002 (Nebraska DMI-0600733), and a subcontract through Ohio State University, NSF EEC-0425626 (RF 60002999). The Coalescence Filtration Nanomaterials Consortium of the University of Akron provided financial support and an industrial point of view. The authors thank Dr. Daniel Galehouse for the design and construction of a laser velocimeter, and Mr. Steven Roberts for technician support. DHR and TH thank Apogee Technology Inc. for financial support. ALY also acknowledges partial support of this work by the National Science Foundation under Grant NIRT CTS-0609062.

References

[1] Taylor GI. Proceedings of the 12th international congress of applied mechanics. Stanford; 1968. p. 382–88.
[2] Timoshenko SP, Gere JM. Theory of elastic stability. NewYork: McGraw-Hill; 1961.
[3] Cruickshank JO, Munson BR. J Fluid Mech 1981;113:221–39.
[4] Cruickshank JO. J Fluid Mech 1988;193:111–27.
[5] Tchavdarov B, Yarin AL, Radev S. J Fluid Mech 1993;253:593–615.
[6] Yarin AL, Tchavdarov B. J Fluid Mech 1996;307:85–99.
[7] Yarin AL. Free liquid jets and films: hydrodynamics and rheology. Harlow, New York: Longman Scientific & Technical, Wiley & Sons; 1993.
[8] Chiu-Webster S, Lister JR. J Fluid Mech 2006;569:89–111.

[9] Ribe NM, Lister JR, Chiu-Webster S. Phys Fluids 2006;18(12): 124105.
[10] Reneker DH, Yarin AL, Fong H, Koombhongse S. J Appl Phys 2000;87(9):4531–47.
[11] Yarin AL, Koombhongse S, Reneker DH. J Appl Phys 2001;89(5):3018–26.
[12] Reneker DH, Yarin AL, Zussman E, Xu H. Adv Appl Mech 2007;41:43–195.
[13] Yarin AL, Kataphinan W, Reneker DH. J Appl Phys 2005;98(6): 064501.
[14] Reneker DH, Han T. Mater Res Soc Symp Proc 2007;948. 0948-B07-01.
[15] Kessick R, Tepper G. Appl Phys Lett 2004;84:4807–9.
[16] Shin MK, Kim SI, Kim SJ. Appl Phys Lett 2006;88:223109.